Published as:
Gok, R., Sandvol, E., Turkelli, N., Seber, D., and Barazangi, M., 2003. Sn attenuation in the Anatolian and Iranian plateau and surrounding regions, *Geophys. Res. Lett.*, 30(24).

Sn attenuation in the Anatolian and Iranian plateau and surrounding regions

Rengin Gök[1], Eric Sandvol[2], Niyazi Türkelli[3], Dogan Seber[4], and Muawia Barazangi[4]

[1]Lawrence Livermore National Laboratory, Livermore, California 94550
[2]Department of Geological Sciences, University of Missouri, Columbia, Missouri 65211
[3]Kandilli Observatory and Earthquake Research Institute, Bogaziçi University, Istanbul, Turkey
[4]Institute for the Study of the Continents, Cornell University, Ithaca, New York 14853

Abstract. The propagation characteristics of the regional Sn shear waves have been mapped to provide insight into the lithospheric structure of the Anatolian and Iranian plateau and the surrounding regions. Thousands of regional earthquakes within the distance range of 2 -15 degrees were recorded by broadband and short period stations located in Turkey and nearby regions, especially new data recorded by 29 broadband stations in the Eastern Turkey Seismic Experiment network. The propagation efficiencies of Sn were determined visually using their amplitude and frequency content. Attenuation maps were then tomographically constructed using the observed propagation efficiencies. Our results confirm that Sn propagates efficiently in the uppermost mantle beneath the Mediterranean Sea, the Black Sea, and the Caspian Sea and along the Zagros fold and thrust belt. Sn is not observed in eastern Turkey, northwestern Iran, or central Anatolia. In contrast to previous available studies, this study considerably improved the mapped location of the boundaries between the zones of efficient and attenuated Sn. Our results are best explained by an absence of lithospheric mantle, or the presence of thin and hot lithospheric mantle beneath most of the Anatolian and Iranian plateau.

Introduction

The tectonics of the northern Middle East is dominated by the collision between the Arabian and Eurasian plates. This continent-continent collision is marked by the Bitlis-Zagros fold and thrust belt; the collision of the Arabian and Eurasian plates began in the mid-Miocene [*Sengör and Yılmaz*, 1981; *Dewey et al.*, 1986]. In the Anatolian plateau, volcanic activity began in the Neogene (8 Ma) and intensified during the Quaternary [*Yılmaz et al.*, 1998], when large volcanic centers developed throughout the Anatolian plateau. Eastern Turkey alkaline and calc-alkaline basalts are known to have originated from the uppermost mantle [*Pearce et al*., 1990]. The Greater and Lesser Caucasus have been tectonically active since the middle to late Pliocene [*Philip et al.*, 1989]. The initiation of continent-continent collision caused the folding and thrusting and uplift of the Greater Caucasus. In the eastern Mediterranean, the African plate is moving northward relative to the Anatolian plate along the Hellenic trench and Cyprean arc [*McKenzie*, 1978]. The African plate is being subducted along the Hellenic arc at a rate of ~40 mm/yr [*Reilinger et al.*, 1997].

The high frequency regional shear wave Sn propagates efficiently through stable lithospheric mantle observed out to distances of 30 degrees. Sn is a leaky mode guided shear wave observed at frequencies of 0.5 Hz up to 20 Hz. Due to its high frequency content, this phase is highly sensitive to the rheology of the mantle lid. The Sn phase is strongly affected when either the lithospheric mantle is hot or there are small amounts of partial melt in the uppermost mantle [*e.g., Ni and Barazangi*, 1983]. *Kadinsky-Cade et al.* [1981] mapped Sn attenuation for the Middle East and found a region of inefficient Sn propagation in the northern part of Anatolia. More recently, *Rodgers et al.* [1997] mapped Sn and Lg attenuation in more detail in the Middle East using the Iranian Long Period Array (ILPA) and five digital broadband stations. *Gök et al*. [2000] and *Sandvol et al.* [2001] extended the Sn

attenuation zone of *Kadinsky-Cade et al.* [1981] in eastern Anatolia to include the entire plateau.

Data and Method

We have used Sn attenuation tomography to quantitatively map regions of Sn blockage throughout the northern Middle East with an emphasis on eastern Turkey. This method used Sn efficiencies from *Gök et al.* [2000] where the amplitude of Sn was compared to the other regional waves (primarily Pg and Lg) and categorized into one of three groups: efficient, inefficient, or not observed. An arrival was classified as 'efficient Sn' if Sn could be clearly observed as high frequency and high amplitude at the phase velocity of 4.5 km/s. If Sn could be seen only on the horizontal components or by a low pass filter we classified it as 'inefficient Sn'. If there was no indication of any phase or amplitude change we classified it as 'no Sn'. In addition to ~2000 seismograms from *Gök et al*. [2000], we used ~700 new waveforms from the Eastern Turkey Seismic Experiment-PASSCAL array (ETSE). We also included some Sn efficiencies from *Sandvol et al.* [2001] in order to obtain better azimuthal coverage throughout the northern part of the Arabian Plate [Figure 1]. Detailed station specifications can be found in *Sandvol et al.* [2001] and *Gök et al.* [2000]. Thousands of waveforms were collected from these stations with varying epicentral distances [Figure 2]. In this study, event locations were obtained from the Preliminary Determination of Epicenters (PDE) monthly catalog and the Kandilli Observatory and Earthquake Research Institute (KOERI) catalog. Seismograms with signal to noise ratios less than three were eliminated. We used seismograms with epicentral distances between 2° and 15°. Vertical and horizontal seismograms were bandpass filtered with corner frequencies of 2 and 5 Hz in addition to a 0.5-5 Hz bandpass filter. Sn has high frequency content and can be more easily observed when using a high pass filter that suppresses some of the longer period energy from

Pg A set of representative waveforms from the ETSE network is shown in Figure 3. We can clearly see the transition from efficient to inefficient or no Sn propagation across the Bitlis suture. One hundred kilometers appears to be sufficient to block Sn propagation entirely in the Anatolian plateau [e.g., waveforms 6 and 7].

Sn attenuation tomography is an objective approach for mapping Sn blockage zones. Using the relation from *Sandvol et al*. [2001] for Sn efficiency and attenuation, we first assume that geometrical spreading or source effects will not significantly contribute to Sn blockage. Following these assumptions, discrete wave propagation efficiencies can be used to obtain the inverse extinction path length for each block in our tomographic parameterization,

$$\Delta A_{ij} = \log_{10}\left(a_{ij}^{0}/a_{ij}\right) = \log_{10} e\,\frac{\pi f}{V_{Sn}}\sum_{n} m_n \ell_{ijn} \qquad (1)$$

ΔA_{ij} is the discrete attenuation factor (i.e., a number representing our qualitatively determined attenuations as percentage attenuation) at the i^{th} station, j^{th} earthquake and n^{th} cell where ℓ is the path length and m is Sn attenuation at the n^{th} block. Following the method outlined in *Sandvol et al.* [2001], we used the LSQR (Least Square) algorithm to invert for the optimal set of extinction path lengths. In order to avoid over or under damping of our solution we performed a large number of tests to determine the optimal damping parameter and cell size. We found that the optimal damping parameter is 0.4 and the optimal cell size is 0.5 degrees.

We defined the three Sn efficiencies in a somewhat ad-hoc manner. In order to test the effect of changing the relative weighting of our qualitative Sn efficiencies differently, we systematically changed the definition of our efficiencies in order to assess the impact on our

tomographic model. We found that the following attenuation percentages best represent our visual inspections. In general we assumed that there is no attenuation for efficient Sn;

$\Delta A_{ij} = 0$ (0 % attenuation) (2)

corresponds to an infinite extinction path length. We used the following definition for inefficient and absent Sn:

$\Delta A_{ij} = 0.5$ Inefficient Sn $a_{ij} / a_{ij}^0 = 0.3$ (70 % attenuation) (3)

$\Delta A_{ij} = 1$ No Sn $a_{ij} / a_{ij}^0 = 0.1$ (90 % attenuation).

By varying the assumed percent attenuation for each efficiency, we can test how robust our tomographic models are using these assumptions. We have found that western Turkey is the region most sensitive to the Sn efficiency definition. This is the region where we observe a large number of inefficient Sn phases.

Because the LSQR algorithm prevents us from calculating a model covariance and resolution matrix, a number of techniques are used to ensure that only well-constrained features are interpreted and that we can reliably estimate the resolution of the attenuation model. We used checkerboard and spike synthetic models to assess the resolution in the Sn attenuation tomography. The synthetic propagation efficiencies are reproduced by defining an extinction path length, which is the propagation distance at which Sn is eliminated, and thus attenuation is complete [*Sandvol et al., 2001*]. The reliability of efficiency models is checked and compared with recovered efficiency model using various synthetic models such as spike and checkerboard. Regions where the recovered model matches the synthetic model are well resolved, whereas a poorly recovered region is considered to be unreliable. We also added 10% noise to the synthetic data by randomly changing the synthetic efficiencies to simulate the effect of misclassification or various complications in the data. The results from

a checkerboard test for an extinction path length of 350 km, which corresponds to Q = 100, are shown in Figure 4b. 5° by 5° synthetic attenuating cells were used in the test. In this example the regions with fewer hit counts had greater smearing of the synthetic anomalies. A number of extinction path lengths, i.e., 150, 350, 500 and 700 km, were used to test the maximum size of features that the ray paths pass through. We were unable to completely recover synthetic anomalies with synthetic extinction path lengths greater than 500 km, although we were able to recover most synthetic anomalies with extinction path lengths between 150 and 500 km. The checkerboard patterns in Figure 4b illustrate the resolution for the Sn ray paths used in this study. Overall, we have good resolution throughout most of Turkey and the northern Middle East; resolution within the Zagros and Gulf regions is considerably less .

Results

The Sn attenuation tomography model is shown in Figure 4a. We have resolved new regions of blocked and significantly attenuated Sn. In the Black Sea there is a very sharp transition from efficient to blocked Sn. Efficient Sn is observed for paths within the eastern Arabian plate and along the Zagros fold and thrust belt. There is an efficient zone seen at the northern part of the Zagros fold and thrust belt in the northwestern corner of Iran. In fact, we observe some clear evidence of efficient Sn propagation within this corner of the Iranian plateau. This anomaly is primarily due to paths with efficient Sn that have traveled from earthquakes in northwestern Iran to stations along the western Caspian and Caucasus mountains. This region of efficient Sn propagation might also be significantly distorted due to lack of resolution in this part of our model [Figure 4b]. Sn is blocked throughout the Anatolian plateau while it propagates efficiently within the eastern part of the Zagros suture. Many paths traveling in the Anatolian plateau did not show any indication of Sn propagation.

We clearly defined the boundaries of efficient Sn in the Black, Mediterranean and Caspian Seas. Using the ETSE data we have substantially improved the resolution of the anomalies in eastern Turkey and the surrounding regions. In general we observe a strong correlation between Quaternary volcanism and Sn blockage. Throughout the entire Anatolian plateau and western Arabian plate there is young basaltic volcanism that clearly correlates with regions of Sn attenuation [Figure 4a]. We also observe a strong correlation between Sn blockage and low Pn velocity regions from the tomographic study of *Al-Lazki et al.* [2003].

In the northeastern portion of our model, inefficient Sn is observed in the Greater Caucasus. Lack of shorter and reciprocal paths may affect the edges of these attenuating regions [Figure 2, Figure 4b]. Throughout most of the Lesser Caucasus, Sn is highly attenuated. Sn is observed as inefficient across much of the Pontides (northern Anatolia). In southwestern Turkey, we observe some inefficient Sn propagation. The inversion results along the eastern Mediterranean Sea show that the upper mantle attenuation zone boundary coincides with the coastline or the transition from oceanic to continental lithosphere.

Discussion and Conclusions

Strong attenuation of Sn beneath the Anatolian and Iranian plateau is a good indication of anomalously hot and thin lithospheric mantle. In western Turkey, we do not observe a distinct high Sn attenuation zone. The Black Sea, the Caspian Sea, and the Mediterranean Sea, that are known to have cold and fast lithospheric mantle, are regions of high amplitude Sn phases typical of oceanic paths [Rodgers et al., 1997; Gök et al.,2000; Sandvol et al., 2001]. The Black Sea was formed by extension during middle to late Mesozoic and there is no indication of a granitic layer under the Black Sea [*Zonenshain and Le Pichon*, 1986]. Efficient Sn propagation within the Black Sea is consistent with the Black Sea lithosphere being oceanic. In central Anatolia, the Neogene volcanism is known to be

derived from upper mantle sources [e.g. Pearce et al., 1989]. A zone of Sn blockage is consistent with the presence of Holocene volcanoes north of the central Taurus Mountains. In the same region, a zone of lower Pn velocities is also observed [*Al-Lazki et al.*, 2003].

Inefficient or no Sn propagation is observed within the western part of the Greater and Lesser Caucasus coinciding with the remnants of back-arc volcanism. Efficient Sn propagation might indicate the presence of cold lithosphere underneath the eastern Greater Caucasus. The Lesser Caucasus, however, is a highly attenuating region similar to the Anatolian plateau. It might be considered to be a continuation of the Anatolian plateau based on the similar attenuating structure within the upper mantle and similarly high topography. Sn propagation is efficient in the stable platform of the Arabian plate; however, Sn is attenuated immediately beneath and to the east of the Dead Sea fault zone (DSFZ). We observe interesting differences between the Pn velocities *(Al-Lazki et al., 2003)* and the Sn attenuation south of the EAFZ (East Anatolian Fault Zone). Sn attenuation is high even though Pn velocities are almost normal. Pn velocity tomography will probably tend to have higher resolution than Sn efficiency tomography; thus that region of relatively normal Pn may be unresolvable by Sn tomography. Even for very short paths we observe no Sn phases in most of eastern Turkey, where continent-continent collision is taking place along the Bitlis suture. The Bitlis suture appears to be a sharp transition from efficient to no Sn propagation in the eastern part of the Arabian plate. This is a clear indication of fundamental differences in the rheology of the upper mantle across the Bitlis suture indicating the lack of any underthrusting of the Arabian plate beneath eastern Turkey. It is important to note that wherever there are Holocene volcanoes we find high Sn attenuation. Since most magma generation appears to be uppermost mantle in origin, this observation is not unexpected. Furthermore this observation is consistent with their being little or no lithospheric mantle

beneath the Anatolian plateau [*Al-Lazki et al*., 2003 and *Sengor et al*., 2003]. Zones of Sn blockage can be due to partial melt within the uppermost mantle (anelastic attenuation) or irregularities in the upper mantle Sn wave guide (scattering attenuation). Comparisons with Pn tomography suggest that most of the attenuation is due to anelasticity; that is, high attenuation corresponds with low velocities. However, in regions where we observe fast to normal Pn velocities and Sn blockage, scattering attenuation may be responsible for the observed Sn blockage. This may be the case for the northwestern corner of the Arabian plate.

The origin of the uppermost hot mantle beneath the world's continental plateaus may be a result of asthenospheric upwelling. This may also be the case beneath the Anatolian plateau, where the observed Sn attenuation is consistent with a model involving the recent break off of the NeoTethys slab and (Keskin, 2003) and an associated asthenospheric upwelling leading to wide spread partial melt throughout the east Anatolian uppermost mantle.

Acknowledgements: We thank Bogaziçi University Kandilli Observatory and Earthquake Research Institute (KOERI), and the Earth Sciences Research Institute of MRC-TUBITAK, for providing us with seismic waveform data. We also thank IRIS for providing waveform data from the GSN stations in the region. The ETSE study was supported by the National Science Foundation under Grant No EAR-9804780. Additional support was provided by the Bogaziçi University Research Fund under Grant No 99T206.

References

Al Lazki, A., E. Sandvol, D. Seber, M. Barazangi and N. Turkelli, Pn tomographic imaging of mantle lid velocity and anisotropy at the junction of the Arabian, Eurasian and African Plates, *Geophys. Res. Lett,* in press, 2003.

Barka, A., and R. Reilinger, Active tectonics of the eastern Mediterranean region: Deduced from GPS, neotectonic and seismicity data, *Annali di Geofisica, 40,* 587-610, 1997.

Burke, K., and C. Sengör, Tectonic escape in the evolution of the continental crust, in *Reflection seismology: The continental crust,* Geodynamics Series Volume 14, edited by M. Barazangi and L. Brown, pp. 41-53, American Geophysical Union, Washington, 1986.

Dewey, J.F., M.R. Hempton, W.S.F. Kidd, F. Saroglu, and A.M.C. Sengör, Shortening of continental lithosphere: The neotectonics of Eastern Anatolia-a young collision zone, in *Collision Tectonics*, edited by M. P. Coward, and A.C. Ries, pp. 3-36, Geol. Soc. London, London, 1986.

Gök, R., N. Türkelli, E. Sandvol, D. Seber and M. Barazangi, Regional wave propagation in Turkey and surrounding regions, *Geophys. Res. Lett.*, 27, No:3, 429-432, 2000

Hearn, T., and J. Ni, Pn velocities beneath continental collision zones: The Turkish-Iranian plateau, *Geophy. J. Int., 117*, 273-283, 1994.

Kadinsky-Cade, K., M. Barazangi, J. Oliver, and B. Isacks, Lateral variation in high-frequency seismic wave propagation at regional distances across the Turkish and Iranian plateaus, *J. Geophys. Res., 86*, 9377-9396, 1981.

Keskin, M.,

McKenzie, D. P., Active tectonics of the Mediterranean region, *Geophy. J. Roy. Astr. Soc., 30*, 109-185, 1972.

McKenzie, D. P., Active tectonics of the Alpine-Himalayan Belt: The Aegean Sea and surrounding regions, *Geophy. J. Roy. Astr. Soc., 55*, 217-254, 1978.

Ni, J., and M. Barazangi, High-frequency seismic wave propagation beneath the Indian Shield, Himalayan Arc, Tibetan Plateau and surrounding regions: High uppermost mantle velocities and efficient Sn propagation beneath Tibet, *Geophy. J. Roy. Astr. Soc.*, 72, 665-689, 1983.

Pearce, J.A., J.F. Bender, S.E. De Long, W.S.F. Kidd, P.J. Low, Y. Guner, F. Saroglu, S. Moorbath, and J.G. Mitchell, Genesis of collision volcanism in eastern Anatolia, Turkey, *J. Volcanol. Geotherm. Res., 44*, 189-229, 1990.

Philip, H., A.Cisternas, A. Gvishiani, and A. Gorshkov, The Caucasus: An actual example of the initial stages of continental collision, *Tectonophysics, 161*, 393-398.

Reilinger, R.E., S.C. McClusky, M.B. Oral, R.W. King, M.N. Toksöz, A.A. Barka, I. Kinik, O. Lenk, and I. Sanlı, Global positioning system measurement at present-day crustal movements in the Arabia-Africa-Eurasia plate collision zone, *J. Geophys. Res., 94*, 9983-9999, 1997.

Rodgers, A.J., J.F. Ni, and T.M. Hearn, Propagation characteristics of short-period Sn and Lg in the Middle East, *Bull. Seism. Soc. Am., 87*, 396-412, 1997.

Sandvol, E., K. Al-Damegh, A. Calvert, D. Seber, M. Barazangi, R. Mohammad, R. Gök, N. Türkelli, and C. Gürbüz, Tomographic imaging of Lg and Sn propagation in the Middle East. *Pure and Applied Geophysics*, 158, 1121-1163, 2001.

Sengör, A.M.C., and Y. Yılmaz, Tethyan evolution of Turkey: A plate tectonic approach, *Tectonophysics, 75*, 181-241, 1981.

Sengör, A.M.C., S. Özeren, T. Genç and E. Zor, East Anatolian High Plateau as a mantle-supported, north-south shortened domal structure, *Geophys. Res. Lett.* in review, 2003.

Yılmaz, Y., Y. Guner, and F. Saroglu, Geology of the Quaternary volcanic centers of the east Anatolia, *J. Volcanol. Geotherm. Res., 85*, 173-210, 1998.

Zonenshain L.P. and X. Le Pichon, Deep basins of the Black Sea and Caspian Sea as remnants of Mesozoic back-arc basins, *Tectonophysics*, 123, 181-211, 1986.

Figure Captions

Figure 1. Map of study area with major tectonic features. Black triangles are seismic stations used in this study. Arrows indicate the plate motions. BZFTB - Bitlis-Zagros Fold and Thrust Belt.

Figure 2. A map of all ray paths used in this study. The line types illustrate the observed Sn efficiencies.

Figure 3. Some representative waveforms. Triangles indicate stations and stars indicate events. The Sn travel time was computed using an upper mantle velocity of 4.5 km/s. The Lg window marks 3.0 km/s to 3.7 km/s group velocities. Solid lines are efficient Sn and dotted lines are blocked Sn. All displayed seismograms are vertical except for those labeled with an asterisk (*), which are transverse component. Waveforms were bandpassed between 0.5-5 Hz. Sn is blocked within a few tens of kilometers in the Anatolian plateau.

Figure 4 (a) Map showing Sn efficiency tomography results. Dark lines are major tectonic boundaries and light lines are national boundaries. **(b)** Resolution test using a synthetic checkerboard for extinction path length of 350 km (Q = 100).

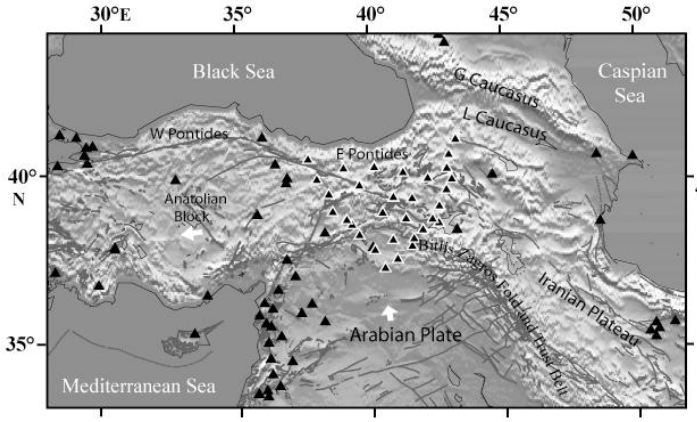

Figure1

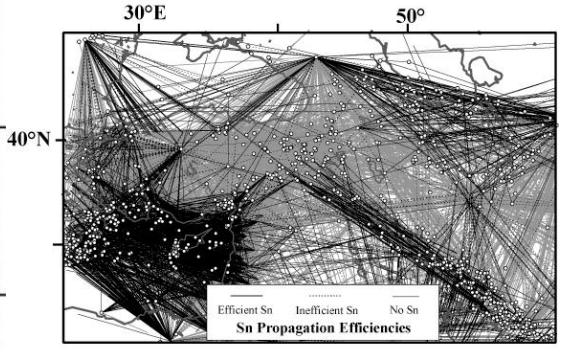

Figure 2

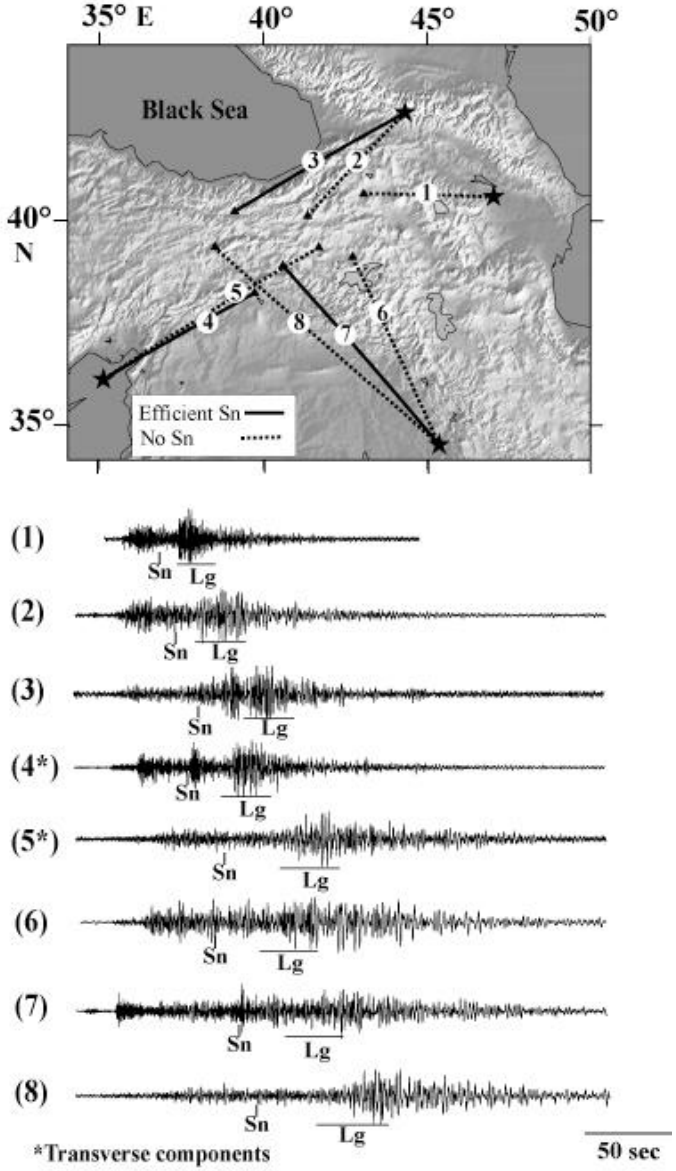

Figure3

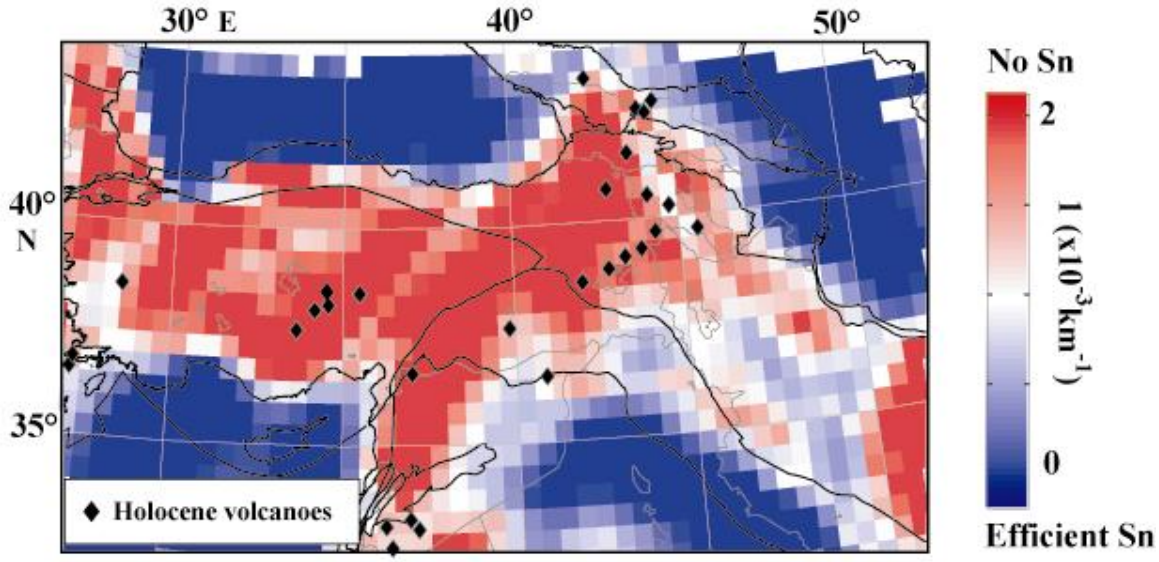

Figure4a

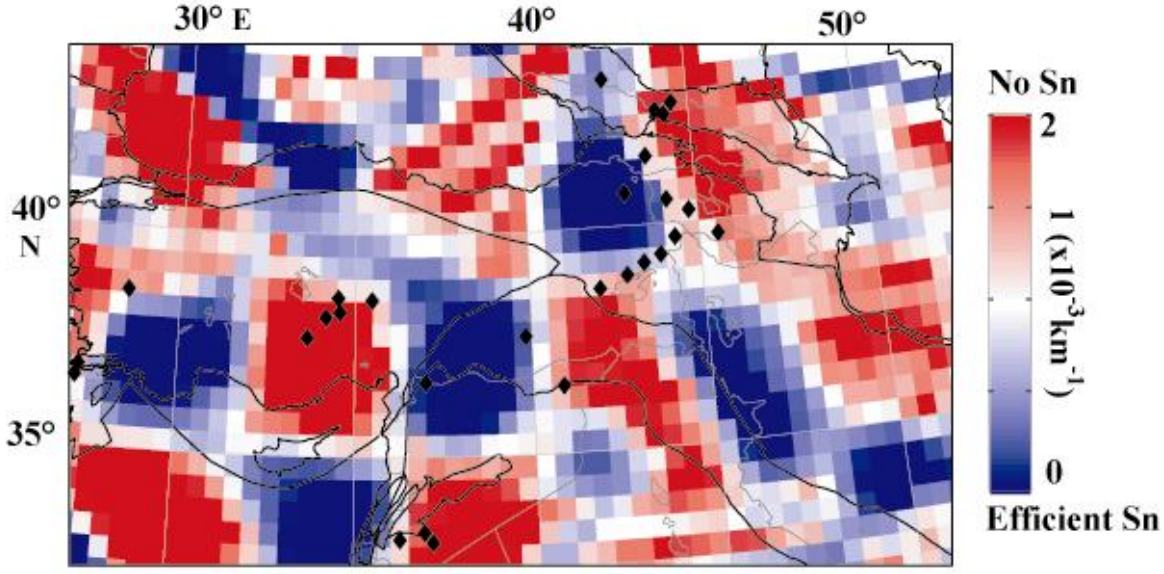

Figure 4b